In Vivo SPECT Imaging of Amyloid-β Deposition with Radioiodinated Imidazo[1,2-*a*]Pyridine Derivative DRM106 in a Mouse Model of Alzheimer's Disease

Chun-Jen Chen[1–3], Kazunori Bando[1], Hiroki Ashino[1], Kazumi Taguchi[1], Hideaki Shiraishi[1], Keiji Shima[1], Osuke Fujimoto[1], Chiemi Kitamura[1], Satoshi Matsushima[1], Keisuke Uchida[1], Yuto Nakahara[1], Hiroyuki Kasahara[1], Takao Minamizawa[1], Cheng Jiang[4], Ming-Rong Zhang[2], Maiko Ono[2], Masaki Tokunaga[2], Tetsuya Suhara[2], Makoto Higuchi[2], Kazutaka Yamada[3], and Bin Ji[2]

[1]Research Department, Fujifilm RI Pharma Co. LTD, Chiba, Japan; [2]Molecular Imaging Center, National Institute of Radiological Sciences, Chiba, Japan; [3]Clinical Veterinary Science, The United Graduate School of Veterinary Science, Gifu University, Gifu, Japan; and [4]School of Pharmacy, Fudan University, Shanghai, China

Noninvasive determination of amyloid-β peptide (Aβ) deposition has important significance for early diagnosis and medical intervention for Alzheimer's disease (AD). In the present study, we investigated the availability of radiolabeled DRM106 ($^{123/125}$I-DRM106 [6-iodo-2-[4-(1*H*-3-pyrazolyl)phenyl]imidazo[1,2-*a*]pyridine]), a compound with sufficient affinity for the synthesis of human Aβ fibrils and satisfactory metabolic stability, as a SPECT ligand in living brains. **Method:** The sensitivity of ^{125}I-DRM106 for detecting Aβ deposition was compared with that of ^{125}I-IMPY (2-(4′-dimethylaminophenyl)-6-iodo-imidazo[1,2-a]pyridine), a well-known amyloid SPECT ligand, by ex vivo autoradiographic analyses in 18-mo-old amyloid precursor protein transgenic mice. To verify the sensitivity and quantitation of radiolabeled DRM106 for in vivo imaging, we compared the detectability of Aβ plaques with ^{123}I-DRM106 and a well-known amyloid PET agent, ^{11}C-labeled Pittsburgh compound B (^{11}C-PiB), in 29-mo-old transgenic mice and age-matched nontransgenic littermates. Additionally, we compared the binding characteristics of ^{125}I-DRM106 with those of ^{11}C-PiB and ^{11}C-PBB3, which selectively bind to Aβ plaques and preferentially to tau aggregates, respectively, in postmortem AD brain sections. **Results:** Ex vivo autoradiographic analysis showed that measurement with ^{125}I-DRM106 has a higher sensitivity for detecting Aβ accumulation than with ^{125}I-IMPY in transgenic mice. SPECT imaging with ^{123}I-DRM106 also successfully detected Aβ deposition in living aged transgenic mice and showed strong correlation ($R = 0.95$, $P < 0.01$) in quantitative analysis for Aβ plaque detection by PET imaging with ^{11}C-PiB, implying that sensitivity and quantitation of SPECT imaging with ^{123}I-DRM106 are almost as good as ^{11}C-PiB PET for the detectability of Aβ deposition. Further, the addition of nonradiolabeled DRM106 fully blocked the binding of ^{125}I-DRM106 and ^{11}C-PiB, but not ^{11}C-PBB3, to AD brain sections, and ^{125}I-DRM106 showed a lower binding ratio of the diffuse plaque–rich lateral temporal cortex to the dense-cored/neuritic plaque–rich hippocampal CA1 area, compared with ^{11}C-PiB. **Conclusion:** All of these data demonstrated the high potential of ^{123}I-DRM106 for amyloid imaging in preclinical and clinical application, and it might more preferentially detect dense-cored/neuritic amyloid deposition, which is expected to be closely associated with neuropathologic changes of AD.

Key Words: Alzheimer's disease (AD); amyloid imaging; amyloid precursor protein (APP) transgenic mouse; DRM106; single photon emission computed tomography (SPECT)

J Nucl Med 2015; 56:120–126
DOI: 10.2967/jnumed.114.146944

Alzheimer's disease (AD) is a progressive neurodegenerative disorder characterized by 2 pathologic hallmarks: amyloid-β peptide (Aβ) plaques and neurofibrillary tangles (NFTs). In vivo noninvasive detection of Aβ deposition is important for early diagnosis and medical intervention of AD at a prodromal stage, because fibrillary Aβ has already been accumulating in the brain for a few decades before AD onset (*1*). Molecular imaging with nuclear medicine technologies such as PET and SPECT is available for both preclinical and clinical use and is considered as a bridge between them. Over the past few years, the availabilities of several PET tracers for amyloid imaging have been successfully verified in AD patients. ^{11}C-labeled Pittsburgh compound B (^{11}C-PiB) is the most widely used PET ligand with which investigators have assessed the longitudinal, quantitative Aβ accumulation in AD model mice and patients (*2–4*) and verified amyloid deposition as a useful imaging biomarker for AD diagnosis, prognostic judgment for conversion from mild cognitive impairment to AD, and evaluation for antiamyloid therapies (*5–7*). To overcome the shortcoming of the limited half-life (~20 min) of ^{11}C-labeled tracers, ligands labeled with ^{18}F (half-life, ~110 min) have also been developed for further routine medical needs (*8–11*).

Although inferior to PET in terms of sensitivity and quantitative performance, SPECT imaging has advantages of operating cost and already-installed rate in medical hospitals, making it more suitable for primary screening for prodromal AD patients. For the past decade, several SPECT ligands have been developed for amyloid imaging. ^{123}I-IMPY (2-(4′-dimethylaminophenyl)-6-iodo-imidazo[1,2-a]pyridine) is a SPECT tracer with high affinity for Aβ fibrils, and in vitro autoradiographic analysis has successfully detected amyloid deposition on brain sections from both AD models

Received Aug. 11, 2014; revision accepted Nov. 3, 2014.
For correspondence or reprints contact: Bin Ji, Molecular Imaging Center, National Institute of Radiological Sciences, 4-9-1, Anagawa, Inage-ku, Chiba-shi, Chiba 263-8555, Japan.
E-mail: kihin@nirs.go.jp
Published online Dec. 4, 2014.

and AD patients (*12–16*). However, preliminary clinical data for ^{123}I-IMPY showed a poor signal-to-noise ratio, making it difficult to distinguish between cognitively normal persons and AD patients, possibly because of insufficient affinity for Aβ fibrils, poor brain permeability, or metabolic instability (*17*). Recently, we developed a series of imidazopyridine compounds for amyloid SPECT imaging and obtained a promising candidate compound, termed DRM106 (6-iodo-2-[4-(1*H*-3-pyrazolyl)phenyl]imidazo[1,2-*a*]pyridine), which has higher affinity for synthetic human Aβ fibrils and metabolic stability. In vitro autoradiography with ^{125}I-labeled DRM106 also successfully detected Aβ plaques in postmortem AD patient brains (*18*). In the present study, we performed in vivo imaging with this newly developed SPECT ligand in living model mice with AD-like amyloid pathology and compared it with ^{11}C-PiB in the detectability of Aβ deposition.

MATERIALS AND METHODS

Radiosynthesis of Radioligands

The radiosynthesis of ^{125}I-DRM106, ^{125}I-IMPY, ^{11}C-PiB, and ^{11}C-PBB3 (2-((1*E*,3*E*)-4-(6-(^{11}C-methylamino)pyridin-3-yl)buta-1,3-dienyl)benzo[*d*]thiazol-6-ol) was performed as described in previous publications (*2,12,18,19*). The radiochemical purity of ^{125}I-DRM106, ^{125}I-IMPY, ^{11}C-PiB, and ^{11}C-PBB3 was greater than 95%, and specific radioactivity was 81.4, 81.4, 93–354, and 72–204 GBq/μmol, respectively, at the end of synthesis.

^{123}I-DRM106 was prepared by the reaction of its precursor with ^{123}I-NaI in the presence of chloramine T (Fig. 1). Briefly, chloramine T (0.035 mg/20 μL 2-propanol) was added to 4.5 mL of 35 mM phosphate buffer (pH 6.3) containing ^{123}I-NaI (29.9 GBq; Fujifilm RI Pharma Co., Ltd. [specific activity was adjusted to 714 GBq/μmol by addition of nonradiolabeled NaI]) and precursor (0.638 mg) and incubated for 5 min at room temperature, followed by quenching by the addition of 200 μL of 1N NaOH. Then the reaction mixture was incubated at 70°C for 30 min and terminated by cooling. The subsequent experimental procedure was the same, with the preparation of ^{125}I-DRM106 as described in our previous publication (*18*). The radiolabeling efficiency of ^{123}I-DRM106 was 65%–80% based on radio–thin-layer chromatography measurement. The radiochemical purity was greater than 95% at the end of synthesis, and the theoretic value of the specific activity was 714 GBq/μmol, considering that the reaction of ^{123}I-NaI and precursor led to the formation of ^{123}I-DRM106 with a 1:1 stoichiometric ratio.

Experimental Animals

A transgenic mouse line (Tg2576), which overexpresses a mutant form of amyloid precursor protein (APPK670/671 L), was purchased from Taconic Farms Inc. Then we generated a JU-Tg2576 mouse by backcrossing of Tg2576 with a JU strain (JU/Ct-C, A.) mouse over 29 generations under license agreement of the Mayo Foundation for Medical Education and Research from Daiichi Sankyo Co. Ltd. for easier daily handling. Transgenic mice (termed JU-Tg2576 if without special description) and body weight–matched nontransgenic JU strain mice as control animals were used in the present study, except for in vivo SPECT imaging, for which commercially available Tg2576 mouse brain was used.

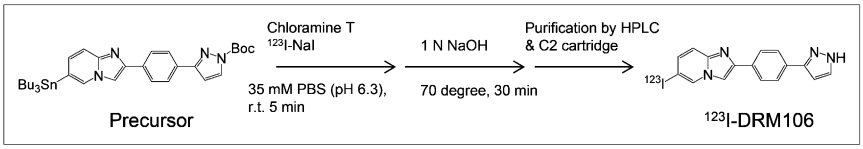

FIGURE 1. Radiosynthesis for ^{123}I-DRM106.

Preparation of Brain Homogenates and Aβ Fibrils, In Vitro Binding Assay and Aβ Assessment, In Vitro and Ex Vivo Autoradiographic Analysis and Metabolite Analysis, and Small-Animal PET and SPECT Imaging

Experimental procedures are presented in the supplemental data (supplemental materials are available at http://jnm.snmjournals.org).

Statistical Analysis

All statistical examinations in the present study were performed by SPSS software (SPSS Inc.). Statistical analyses for group comparisons were performed by Student *t* test or ANOVA followed by Bonferroni post hoc test. The correlation between 2 parameters was examined by parametric test with Pearson product-moment correlation coefficient (R). The difference between groups was considered significant at a P value less than 0.05. All data were expressed as mean ± SD.

RESULTS

In Vitro Binding of DRM106

Saturation curves and Scatchard analyses using a 2-site binding model demonstrated that the dissociation constant (K_d) values of high-affinity binding sites of DRM106 to synthetic human Aβ(1–40) and Aβ(1–42) fibrils, brain homogenates of transgenic mice, and AD patients were approximately 1–10 nM, and the K_d values of low-affinity sites were approximately 100–300 nM (Supplemental Fig. 1; Table 1). To estimate the correlation between quantitative ^{125}I-DRM106 binding and Aβ amounts, brain homogenates of transgenic mice at different ages (8.1–17 mo) were used for the measurement of ^{125}I-DRM106 binding and Aβ amounts. Age-dependent increases in ^{125}I-DRM106 binding and Aβ amounts were detected, and there was excellent correlation between ^{125}I-DRM106 binding and the amount of either Aβ(1–40) ($R = 1$, $P < 0.01$) or Aβ(1–42) ($R = 0.99$, $P < 0.01$) (Fig. 2).

Metabolite Analysis in Transgenic Mice

Solutions of ^{125}I-DRM106 (1.1 MBq) were injected into male JU-Tg2576 transgenic mice (age, 18 mo) via the tail vein, and metabolite analyses were performed as described in our previous publication (*18*). Similar to results in normal rats (*18*), there were no detectable metabolites in the brain over the observation period, whereas only a little metabolite-related radioactivity was observable in the plasma samples, in addition to unchanged ^{125}I-DRM106 (Fig. 3).

Ex Vivo Autoradiography with ^{125}I-DRM106 and ^{125}I-IMPY

The sensitivity of ^{125}I-DRM106 for detecting Aβ plaques was higher than that of ^{125}I-IMPY, based on the experimental observation that more amyloid plaques were detectable using ^{125}I-DRM106 than ^{125}I-IMPY at 3 indicated time points in 18-mo-old transgenic mice (Fig. 4). Meanwhile, no overt difference in amyloid deposition labeled by congo red was detectable between 2 experimental groups for ^{125}I-DRM106 and ^{125}I-IMPY analysis (data not shown). Although slight nonspecific binding of ^{125}I-DRM106 to white matter was detectable in both transgenic and nontransgenic mice at 1 h after injection, background radioactivity decreased to an undetectable level after 2 h (Fig. 4A), suggesting that the optimum scan time for in vivo imaging with radiolabeled DRM106 was between 1 and 2 h for acquiring good contrast with minimum loss in radioactive signals. Ex vivo emulsion autoradiography and consequent fluorescent labeling with thioflavin-S showed great consistency of ^{125}I-DRM106

TABLE 1
Binding Parameters of ^{125}I-DRM106

Sample	High-affinity binding site			Low-affinity binding site		
	K_d*	B_{max}†	BP‡	K_d	B_{max}	BP
Aβ(1–40) fibrils (n = 4)	1.50 ± 0.00	4.30 ± 1.00	—	1,400 ± 36.6	163 ± 9.60	—
Aβ(1–42) fibrils (n = 4)	10.1 ± 5.10	34.3 ± 22.8	—	2,890 ± 344.5	339 ± 268	—
Transgenic brain (n = 4)	4.20 ± 0.92	113 ± 133	26.9	264 ± 160	3,780 ± 1,008	14.3
AD brain	4.30 ± 1.20	681 ± 305	158.4	101 ± 37.8	7,050 ± 1,985	69.8

*K_d is expressed as nmol/L.
†B_{max} for Aβ fibrils and mouse/human tissues is expressed as pmol/nmol of Aβ and pmol/g of tissue.
‡BP = B_{max}/K_d.
Data of Aβ fibrils were from 4 independent experiments, and each experiment was run in triplicate. Data of transgenic brains were from 4 mice (20 mo old), and each experiment was run in triplicate. Data of AD brain were from triplicate experiments. Data are mean ± SD.
B_{max} = maximum binding value; mo = month.

accumulation and thioflavin-S–positive Aβ deposition (Supplemental Fig. 2).

In Vivo Imaging with ^{123}I-DRM106 SPECT and ^{11}C-PiB PET

To investigate the capacity of ^{123}I-DRM106 for in vivo detection of amyloid deposition, we performed in vivo imaging with ^{123}I-DRM106 and ^{11}C-PiB in the same mice and compared their quantitative analysis. The accumulation of ^{11}C-PiB in the frontal/parietal cortex and hippocampus regions enriched with amyloid deposition was more abundant than that in other brain regions in transgenic mice (Tg2576), whereas no regional difference in radioactivity accumulation was detectable in age-matched nontransgenic mice. In vivo images of ^{123}I-DRM106 showed great similarity to those of ^{11}C-PiB except for more intelligible accumulation in the cerebellum (Fig. 5A; Supplemental Fig. 3). Subsequent ex vivo autoradiography also clearly demonstrated consistency in radioligand accumulation with the observation of in vivo imaging. Quantitative analysis showed that both ^{11}C-PiB and ^{123}I-DRM106 accumulations in amyloid pathology–enriched regions (cortex/hippocampus) in transgenic mice were significantly higher than in nontransgenic mice (Fig. 5B). Positive correlations between amyloid depositions detected by these 2 radioligands (R = 0.95, $P < 0.01$) and between in vivo and ex vivo binding of ^{123}I-DRM106 (R = 0.98, $P < 0.01$) were statistically significant (Fig. 5C). Although using cerebellum with slight to moderate amyloid pathology as reference tissue would underestimate the binding potential (BP) calculated from the simplified reference tissue model, this would not affect our correlation analysis.

Binding of ^{125}I-DRM106, ^{11}C-PiB, and ^{11}C-PBB3 in Postmortem Human Brain

To evaluate binding sites of ^{125}I-DRM106 in AD brain, we compared the in vitro autoradiographic images of ^{125}I-DRM106 with ^{11}C-PiB or ^{11}C-PBB3, a radiolabeled ligand that binds to both amyloid and tau lesions at 5 nM of incubation concentration (*19*), in AD brain sections containing the hippocampus and lateral temporal cortex (LTCx) regions. The addition of nonradiolabeled DRM106 fully blocked the binding of ^{125}I-DRM106 and ^{11}C-PiB, and partially ^{11}C-PBB3, in AD brain sections (Fig. 6A). ^{125}I-DRM106, ^{11}C-PiB, and ^{11}C-PBB3 showed detectable specific binding in LTCx regions harboring numerous plaques including dense-cored/neuritic and diffuse plaques and NFTs, and in the hippocampal CA1 sector enriched with NFTs and Aβ deposition composed of numerous dense-cored/neuritic and few diffuse plaques, to greater or lesser degrees (Figs. 6B and 6C; Supplemental Fig. 4). The LTCx-to-CA1 ratio of ^{125}I-DRM106 binding was similar to that of ^{11}C-PBB3 but significantly lower than that of ^{11}C-PiB (Fig. 6D).

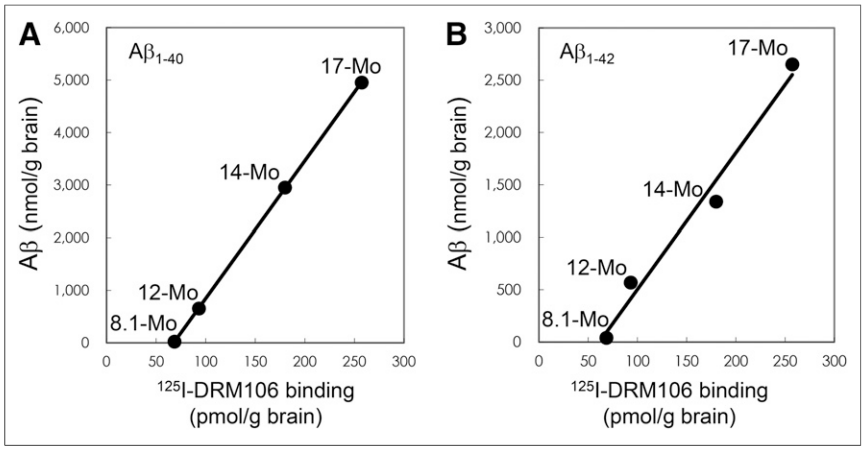

FIGURE 2. Correlation between amounts of Aβ species and binding of ^{125}I-DRM106. ^{125}I-DRM106 binding and amounts of Aβ were increased age-dependently in brain homogenates of transgenic mice at different ages as indicated, and correlations between ^{125}I-DRM106 binding and Aβ(1–40) (A) and Aβ(1–42) (B) amounts were statistically significant. Data were from average of triplicate experiments for each age group.

DISCUSSION

For development of a SPECT ligand for amyloid imaging, the compound IMPY is a good guide because it is the first SPECT imaging agent to be tested in human subjects, and a great deal of data have already been published for reference. In vitro autography with ^{123}I-IMPY clearly demonstrated its availability for visualization of Aβ plaques in either AD model (APP/PS1 double-transgenic mouse) or postmortem brain sections. Ex vivo autographic analysis also visually confirmed ^{123}I-IMPY–labeled Aβ plaques in aged APP/PS1 double-transgenic mice (*12*). The

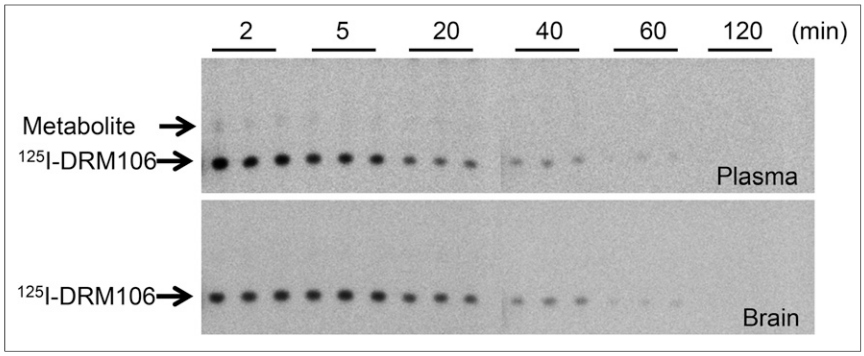

FIGURE 3. Metabolic stability of ^{125}I-DRM106 in transgenic mice. Plasma and brain samples were collected at indicated time points after intravenous injection of ^{125}I-DRM106. Thin-layer chromatography analysis clearly demonstrated that no overt metabolite in brain (lower) and only a little metabolite in plasma (upper) were detectable at the initial phase during observation period.

results of in vivo imaging with micro-SPECT, however, were not encouraging (*17*). Subsequent clinical studies also showed that the signal-to-noise ratio for plaque labeling was not as high as that of ^{11}C-PiB (*17*), indicating that successful development will require higher criteria as exemplified by higher metabolic stability and affinity for Aβ plaques than IMPY. The present and previous data clearly demonstrated that ^{125}I-DRM106 has satisfactory metabolic stability in rodents and higher affinity for synthetic human Aβ fibrils than IMPY (*18*). There was high-level specific binding of ^{123}I-DRM106 to Aβ deposition in Tg2576 mouse and postmortem AD patient brains with high affinity (K_d of 1-digit nM). This characteristic was similar to that of ^{11}C-PiB, as published in a previous study, at low nanomolar concentrations typically used in SPECT studies (*20*). Such improvements in the properties of imaging agents are responsible for the superiority of ^{125}I-DRM106 in the detectability of Aβ plaques, compared with ^{125}I-IMPY, as shown in ex vivo autoradiographic analysis (Fig. 4).

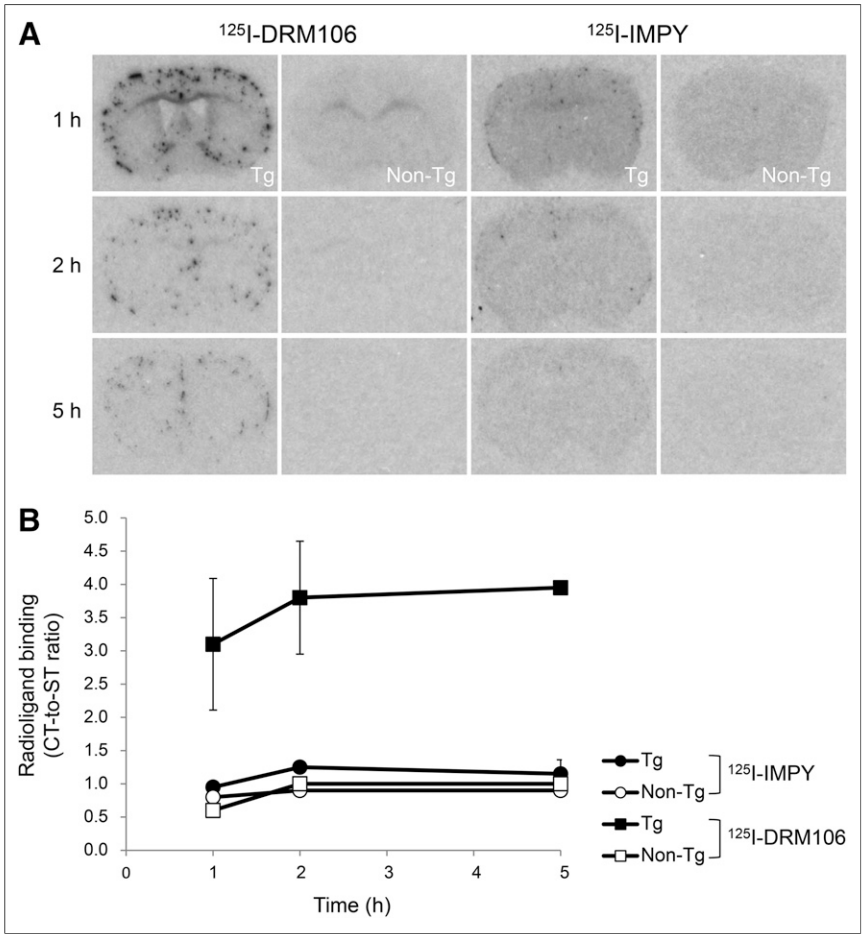

FIGURE 4. Ex autoradiographic analysis of ^{125}I-DRM106 and ^{125}I-IMPY in transgenic mouse brain. (A) Representative coronal images of 18-mo-old male transgenic (from left, first and third columns) and body weight–matched nontransgenic (from left, second and fourth columns) mice administered bolus injection of radiolabeled ^{125}I-DRM106 (from left, first and second columns) and ^{125}I-IMPY (from left, third and fourth columns) at 1, 2, and 5 h after injection. (B) Amyloidosis-associated accumulations of radioligands were quantified as ratios of radioactivity of neocortex to striatum. Data were from experiments shown in A. Transgenic (closed symbols, $n = 2$ for each time point) and nontransgenic (open symbols, $n = 1$ for each time point) mice were administered ^{125}I-DRM106 (squares) and ^{125}I-IMPY (circles). Data are mean ± SD. CT = neocortex; Non-Tg = nontransgenic; ST = striatum; Tg = transgenic.

Recently, amyloid deposition in 28-mo-old Tg2576 mice was successfully visualized with a radioiodine-labeled pyridyl benzofuran derivative (*21*). There was, however, relatively high retention, approximately 40% of initial brain uptake, in the normal brain even after 60 min and resulting high-level nonspecific binding to white matter (*21*). Given that white matter in human subjects is much more abundant than in rodents, such high-level nonspecific binding to white matter may overtly affect the detectability of Aβ plaques in human subjects. Additionally, this radioligand was not metabolically stable in normal mice. The intact form in plasma was decreased to approximately 20% at 30 min after injection (*21*), raising the undesirable possibility that these radioactive metabolites penetrated into the brain and lowered the signal-to-noise ratio. In contrast, the amount of ^{125}I-DRM106 remaining in the normal brain was lowered to less than 4% of initial uptake after 60 min, exhibiting excellent off-target washout (*18*). As a result, there was low nonspecific binding in white matter and other brain regions without amyloid pathology (Figs. 4 and 5). Additionally, a recent poster presentation—at the Alzheimer Association International Conference (*22*), during which a newly developed radioiodinated tracer, ^{123}I-ABC577, was reported—demonstrated the possible availability of image-based diagnosis for AD in human subjects. Although this is a preliminary result and there is still a lack of accurate information available, such as the chemical structure of ABC577, this successful case has proved the feasibility of this SPECT agent for amyloid imaging in human subjects.

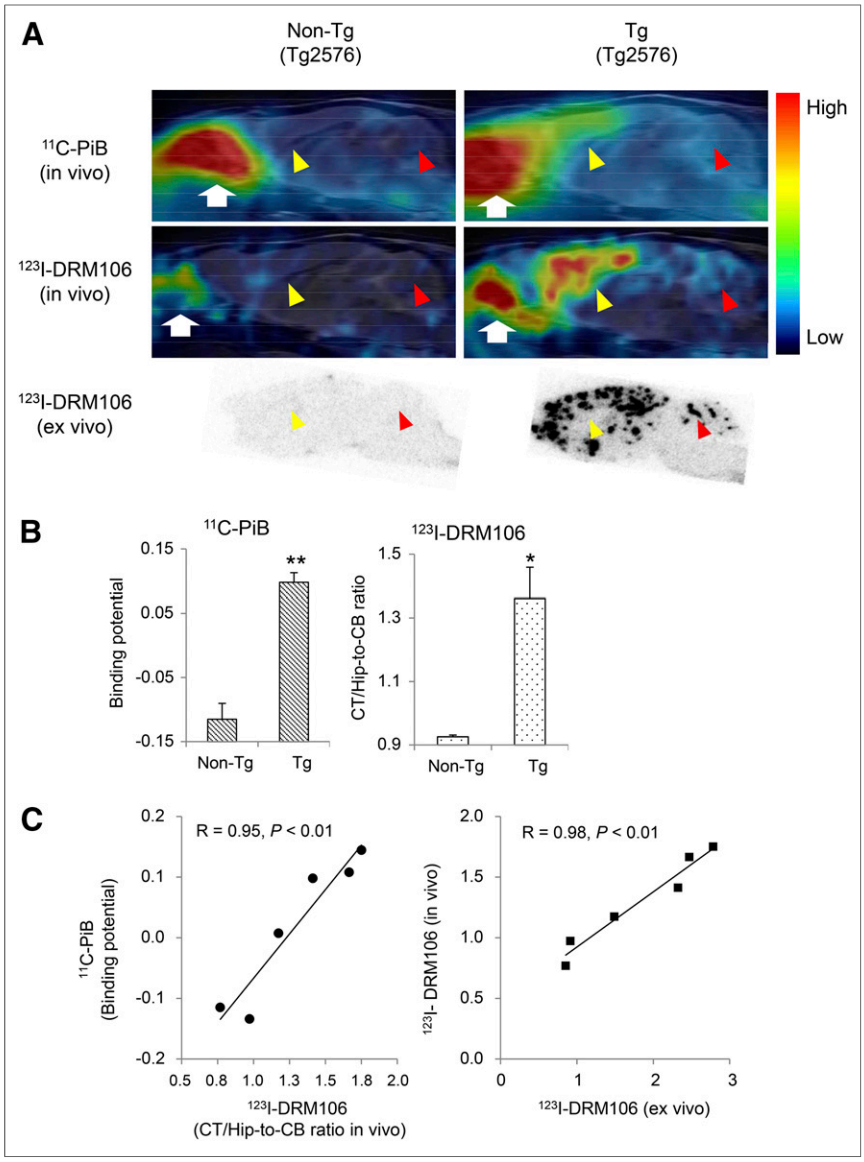

FIGURE 5. In vivo imaging with ^{123}I-DRM106 and ^{11}C-PiB. (A) Typical in vivo images of ^{11}C-PiB (top) and ^{123}I-DRM106 (middle) and ex vivo images of ^{123}I-DRM106 (bottom) in 28-mo-old female transgenic (Tg2576; right) and age-matched nontransgenic littermate (left) mouse brains. In vivo images were overlaid on MR imaging template. Red and yellow arrowheads indicate cerebellum and cortex/hippocampus regions, respectively. White arrows indicate harderian gland. (B) Quantitative analysis for in vivo binding of ^{11}C-PiB and ^{123}I-DRM106 in nontransgenic (n = 3) and transgenic (n = 5) mice. In vivo bindings of ^{11}C-PiB and ^{123}I-DRM106 were estimated by BP and cortex-to-cerebellum ratio, respectively. Data are mean ± SD. *P < 0.05 and **P < 0.01 vs. nontransgenic mouse, t test. (C) Correlation of in vivo binding between ^{11}C-PiB and ^{123}I-DRM106 (left) and between in vivo and ex vivo binding of ^{123}I-DRM106 (right). Data of mice that underwent both ^{11}C-PiB and ^{123}I-DRM106 scans were used for correlation analysis. Non-Tg = nontransgenic; Tg = transgenic.

In comparison with PET, radioisotopes used in SPECT, such as ^{123}I (half-life, 13.22 h), have a longer half-life and can therefore achieve longer distance delivery and cheaper operating cost, and more SPECT scanners have also been installed for routine clinical examinations, making it more suitable for primary screening for prodromal AD patients, especially in developing countries with large territories. Given that the sensitivity and quantitative ability of SPECT are inferior to those of PET, we need more in vivo imaging data to support the availability of DRM106 for further clinical application. We performed in vivo imaging with ^{123}I-DRM106 in Tg2576 mice and compared this with PET imaging with ^{11}C-PiB. Tg2576 is a widely used transgenic mouse line with AD-like amyloid pathology, with Aβ plaque density increasing exponentially from 12 mo, reaching levels similar to those seen in the AD brain (*23*). There were, however, many fewer amyloid-associated binding sites for ^{11}C-PiB in the Tg2576 mouse than in AD patient tissues (*2,24*). Despite the fewer binding sites for ^{11}C-PiB in Tg2576 mice, we successfully detected significant amyloid-associated ^{11}C-PiB accumulation in the living brains, taking advantage of the high-quality ^{11}C-PiB with high specific radioactivity up to approximately 300 GBq/umol, 6–10 times higher than the usually used level, and elderly mice (29 mo). Our comparative analysis showed great consistency in the quantitative detection of Aβ deposition between ^{123}I-DRM106 and ^{11}C-PiB, demonstrating that SPECT imaging with ^{123}I-DRM106 has quantitative ability and sensitivity similar to those of PET with ^{11}C-PiB in the living brain.

On the basis of our experimental result that the LTCx-to-CA1 ratio of binding of ^{125}I-DRM106 is significantly lower than that of ^{11}C-PiB, different pathologic aggregates are expected to provide major binding sites for ^{125}I-DRM106 and ^{11}C-PiB. Although the LTCx-to-CA1 ratio of binding of ^{125}I-DRM106 was similar to that of ^{11}C-PBB3, which binds to both Aβ and tau aggregates at the incubation concentration used (*19*), NFTs might not provide binding sites for ^{125}I-DRM106, because a high concentration of nonradiolabeled DRM106 failed to fully block the binding of ^{11}C-PBB3 when we postulated that NFTs provide similar binding sites for all of the β-sheet ligands. Thus, a reasonable explanation is that ^{125}I-DRM106 might preferentially bind to dense-cored/neuritic plaques as did other amyloid tracers such as ^{18}F-(fluorinated amyloid imaging compound of Tohoku University) (*25*). Given that ^{11}C-PiB also binds to diffuse plaques, in addition to dense-cored/neuritic plaques, the lower LTCx-to-CA1 ratio of binding of ^{125}I-DRM106 than ^{11}C-PiB is consistent with the distribution of Aβ plaques—that is, the major Aβ deposition is dense-cored/neuritic plaques in CA1. In contrast, in addition to dense-cored/neuritic plaques, numerous diffuse plaques are also observed in the LTCx region.

The correlation between PiB binding and the amounts of either Aβ(1–40) or Aβ(1–42) was not significant (*20*), being attributable to preferential binding of PiB to certain Aβ subtypes, such as $A\beta_{N3(pE)}$ (*2*). In contrast, ^{125}I-DRM106 binding showed excellent linearity with the amounts of either Aβ(1–40) or Aβ(1–42) in

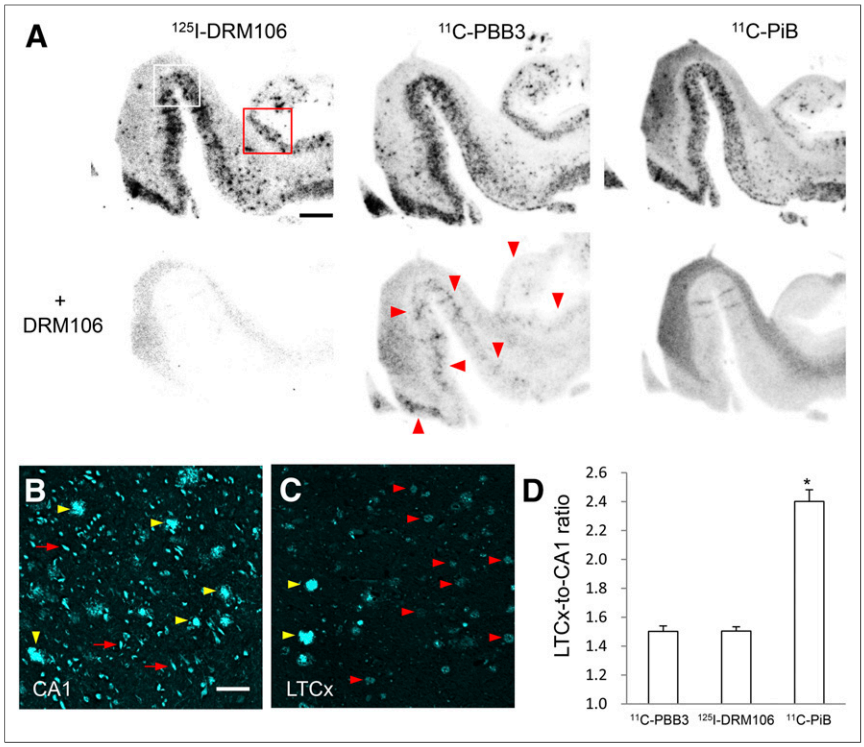

FIGURE 6. In vitro autoradiographic analyses with ^{125}I-DRM106, ^{11}C-PiB, and ^{11}C-PBB3 in postmortem AD brains. (A) Autoradiographic images of ^{125}I-DRM106 (left), ^{11}C-PBB3 (middle), and ^{11}C-PiB (right) and in absence (upper) or presence (lower) of nonradiolabeled DRM106 in brain sections from patient with AD. Slices contain hippocampus, parahippocampal gyrus, and fusiform gyrus. Areas outlined with white and red squares contain hippocampal CA1 and LTCx flanking collateral sulcus, respectively, and high-power images of these 2 regions are shown in Supplemental Fig. 4. Red arrowheads indicate putative NFT-associated binding of ^{11}C-PBB3. (B and C) Fluorescent counterstaining of NFTs (red arrows) and dense-cored/neuritic (yellow arrowheads) and diffuse (red arrowheads) plaques with FSB ((E,E)-1-fluoro-2,5-bis-(3-hydroxycarbonyl-4-hydroxy)styrylbenzene) in CA1 (B) and LTCx (C) regions. (D) Serial brain sections (5, 4, and 4 randomized sections for analyses of ^{125}I-DRM106, ^{11}C-PiB, and ^{11}C-PBB3, respectively) from patient with AD were used for quantitative analyses of specific bindings of these radiolabeled ligands. There was significant main effect ($F_{(2,\ 10)} = 6.32$, $P < 0.05$ by 1-way ANOVA). Post hoc analysis revealed that LTCx-to-CA1 ratio of ^{11}C-PiB was significantly higher than those of ^{125}I-DRM106 and ^{11}C-PBB3 (*$P < 0.05$, Bonferroni). Data are mean ± SD. Scale bars: A, 5 mm; B, C, 50 μm.

Tg2576 brain homogenates, suggesting that the terminal modification of Aβ may not change its binding sites for ^{125}I-DRM106. If so, binding sites for ^{125}I-DRM106 in AD patients and experimental animal models are more similar to each other, compared with that for ^{11}C-PiB. As evidence, the ratio of maximum binding values of ^{125}I-DRM106 for high-affinity binding sites in a 20-mo-old Tg2576 mouse to that in AD brain was proximately 0.17, much higher than that of ^{11}C-PiB (ratio of maximum binding values in a 15-mo-old APP/PS1 double-transgenic mouse to AD brain was below 0.001) (*20*). On the basis of the BP values for high- and low-affinity binding sites in Tg2576 mouse brain being approximately 27 and 14, respectively, the percentage of BP for high-affinity binding is approximately 65%. Likewise, the percentage of BP for high-affinity binding in AD brain is approximately 69% (Table 1). These 2 similar values may imply a similarity of composition of binding sites for ^{125}I-DRM106 in Tg2576 and AD brains, largely differing from that seen in ^{11}C-PiB binding to the AD model mouse and patient brains (percentage of BP for high-affinity binding was ~37% and 92% in the AD model mouse and patient brains, respectively) (*20*). This similarity in values suggests that $^{123/125}$I-DRM106 is more suitable than ^{11}C-PiB for translational research of the progression of amyloid pathology when using existing APP transgenic mouse models, most of which express numerous dense-cored, but not AD-like, diffuse plaques.

CONCLUSION

In this study, we have successfully captured Aβ deposition in a living AD model mouse with a newly developed SPECT agent, ^{123}I-DRM106. Given that its capacity was not inferior to ^{11}C-PiB for detecting Aβ deposition, ^{123}I-DRM106 has a high potential for further clinical application and, in fact, might preferentially capture the deposition of dense-cored/neuritic plaques.

DISCLOSURE

The costs of publication of this article were defrayed in part by the payment of page charges. Therefore, and solely to indicate this fact, this article is hereby marked "advertisement" in accordance with 18 USC section 1734. This work was supported in part by grants-in-aid for Japan Advanced Molecular Imaging Program and Core Research for Evolutional Science and Technology and Scientific Research on Innovative Areas ("Brain Environment") 23111009 from the Ministry of Education, Culture, Sports, Science and Technology, Japan. No other potential conflict of interest relevant to this article was reported.

ACKNOWLEDGMENTS

We thank John Q. Trojanowski and Virginia M.-Y. Lee (Center for Neurodegenerative Disease Research, University of Pennsylvania) for kindly providing human tissue.

REFERENCES

1. Braak H, Braak E. Neuropathological staging of Alzheimer-related changes. *Acta Neuropathol (Berl).* 1991;82:239–259.
2. Maeda J, Ji B, Irie T, et al. Longitudinal, quantitative assessment of amyloid, neuroinflammation, and anti-amyloid treatment in a living mouse model of Alzheimer's disease enabled by positron emission tomography. *J Neurosci.* 2007; 27:10957–10968.
3. Klunk WE, Engler H, Nordberg A, et al. Imaging brain amyloid in Alzheimer's disease with Pittsburgh Compound-B. *Ann Neurol.* 2004;55:306–319.
4. Engler H, Forsberg A, Almkvist O, et al. Two-year follow-up of amyloid deposition in patients with Alzheimer's disease. *Brain.* 2006;129:2856–2866.
5. Ikonomovic MD, Klunk WE, Abrahamson EE, et al. Post-mortem correlates of in vivo PiB-PET amyloid imaging in a typical case of Alzheimer's disease. *Brain.* 2008;131:1630–1645.
6. Leinonen V, Alafuzoff I, Aalto S, et al. Assessment of β-amyloid in a frontal cortical brain biopsy specimen and by positron emission tomography with carbon 11-labeled Pittsburgh Compound B. *Arch Neurol.* 2008;65:1304–1309.
7. Okello A, Koivunen J, Edison P, et al. Conversion of amyloid positive and negative MCI to AD over 3 years: an ^{11}C-PIB PET study. *Neurology.* 2009;73: 754–760.
8. Zhang W, Kung MP, Oya S, et al. ^{18}F-labeled styrylpyridines as PET agents for amyloid plaque imaging. *Nucl Med Biol.* 2007;34:89–97.

9. Choi SR, Golding G, Zhuang Z, et al. Preclinical properties of ^{18}F-AV-45: a PET agent for Aβ plaques in the brain. *J Nucl Med.* 2009;50:1887–1894.
10. Hampel H, Wilcock G, Andrieu S, et al. Biomarkers for Alzheimer's disease therapeutic trials. *Prog Neurobiol.* 2011;95:579–593.
11. Cselényi Z, Jonhagen ME, Forsberg A, et al. Clinical validation of ^{18}F-AZD4694, an amyloid-β-specific PET radioligand. *J Nucl Med.* 2012;53:415–424.
12. Kung MP, Hou C, Zhuang ZP, et al. Characterization of IMPY as a potential imaging agent for β-amyloid plaques in double transgenic PSAPP mice. *Eur J Nucl Med Mol Imaging.* 2004;31:1136–1145.
13. Kung MP, Hou C, Zhuang ZP, et al. IMPY: an improved thioflavin-T derivative for in vivo labeling of β-amyloid plaques. *Brain Res.* 2002;956:202–210.
14. Hsiao IT, Huang CC, Hsieh CJ, et al. Correlation of early-phase ^{18}F-florbetapir (AV-45/Amyvid) PET images to FDG images: preliminary studies. *Eur J Nucl Med Mol Imaging.* 2012;39:613–620.
15. Newberg AB, Wintering NA, Plossl K, et al. Safety, biodistribution, and dosimetry of ^{123}I-IMPY: a novel amyloid plaque-imaging agent for the diagnosis of Alzheimer's disease. *J Nucl Med.* 2006;47:748–754.
16. Song PJ, Bernard S, Sarradin P, et al. IMPY, a potential β-amyloid imaging probe for detection of prion deposits in scrapie-infected mice. *Nucl Med Biol.* 2008;35:197–201.
17. Kung MP, Weng CC, Lin KJ, et al. Amyloid plaque imaging from IMPY/SPECT to AV-45/PET. *Chang Gung Med J.* 2012;35:211–218.
18. Chen CJ, Bando K, Ashino H, et al. Synthesis and biological evaluation of novel radioiodinated imidazopyridine derivatives for amyloid-β imaging in Alzheimer's disease. *Bioorg Med Chem.* 2014;22:4189–4197.
19. Maruyama M, Shimada H, Suhara T, et al. Imaging of tau pathology in a tauopathy mouse model and in Alzheimer patients compared to normal controls. *Neuron.* 2013;79:1094–1108.
20. Klunk WE, Lopresti BJ, Ikonomovic MD, et al. Binding of the positron emission tomography tracer Pittsburgh compound-B reflects the amount of amyloid-β in Alzheimer's disease brain but not in transgenic mouse brain. *J Neurosci.* 2005;25:10598–10606.
21. Ono M, Cheng Y, Kimura H, et al. Development of novel ^{123}I-labeled pyridyl benzofuran derivatives for SPECT imaging of β-amyloid plaques in Alzheimer's disease. *PLoS ONE.* 2013;8:e74104.
22. Maya Y, Okumura Y, Onishi T, et al. Preclinical and clinical properties of [123I] ABC557: a novel radioiodinated SPECT agent for imaging b-amyloid in the brain. Poster presented at: Alzheimer Association International Conference; July 12–16, 2014; Copenhagen, Denmark.
23. Kawarabayashi T, Younkin LH, Saido TC, et al. Age-dependent changes in brain, CSF, and plasma amyloid β protein in the Tg2576 transgenic mouse model of Alzheimer's disease. *J Neurosci.* 2001;21:372–381.
24. Snellman A, Rokka J, Lopez-Picon FR, et al. Pharmacokinetics of [^{18}F]flutemetamol in wild-type rodents and its binding to β amyloid deposits in a mouse model of Alzheimer's disease. *Eur J Nucl Med Mol Imaging.* 2012;39:1784–1795.
25. Ito H, Shinotoh H, Shimada H, et al. Imaging of amyloid deposition in human brain using positron emission tomography and [^{18}F]FACT: comparison with [^{11}C]PIB. *Eur J Nucl Med Mol Imaging.* 2014;41:745–754.